Multipronged Design of Light-Triggered Nanoparticles To Overcome Cisplatin Resistance for Efficient Ablation of Resistant Tumor

Yanli Li,[†,⊥] Yibin Deng,[†,⊥] Xin Tian,[‡,⊥] Hengte Ke,[*,†] Miao Guo,[†] Aijun Zhu,[†] Tao Yang,[†] Zhengqing Guo,[‡] Zhishen Ge,[§] Xiangliang Yang,[∥] and Huabing Chen[*,†,‡]

[†]Jiangsu Key Laboratory of Translational Research and Therapy for Neuro-Psycho-Diseases, and College of Pharmaceutical Sciences, Soochow University, Suzhou, Jiangsu 215123, China, [‡]School for Radiological & Interdisciplinary Sciences (RAD-X), Collaborative Innovation Center of Radiation Medicine of Jiangsu Higher Education Institutions, and School of Radiation Medicine and Protection, Soochow University, Suzhou, Jiangsu 215123, China, [§]CAS Key Laboratory of Soft Matter Chemistry, Department of Polymer Science and Engineering, University of Science and Technology of China, Hefei, Anhui 230026, China, and [∥]National Engineering Research Center for Nanomedicine, and College of Life Science and Technology, Huazhong University of Science and Technology, Wuhan, Hubei 430074, China. [⊥]These authors contributed equally to this work.

ABSTRACT Chemotherapeutic drugs frequently encounter multiple drug resistance in the field of cancer therapy. The strategy has been explored with limited success for the ablation of drug-resistant tumor *via* intravenous administration. In this work, the rationally designed light-triggered nanoparticles with multipronged physicochemical and biological features are developed to overcome cisplatin resistance *via* the assembly of Pt(IV) prodrug and cyanine dye (Cypate) within the copolymer for efficient ablation of cisplatin-resistant tumor. The micelles exhibit good photostability, sustained release, preferable tumor accumulation, and enhanced cellular uptake with reduced efflux on both A549 cells and resistant A549R cells. Moreover, near-infrared light not only triggers the photothermal effect of the micelles for remarkable photothermal cytotoxicity, but also leads to the intracellular translocation of the micelles and reduction-activable Pt(IV) prodrug into cytoplasm through the lysosomal disruption, as well as the remarkable inhibition on the expression of a drug-efflux transporter, multidrug resistance-associated protein 1 (MRP1) for further reversal of drug resistance of A549R cells. Consequently, the multipronged effects of light-triggered micelles cause synergistic cytotoxicity against both A549 cells and A549R cells, and thus efficient ablation of cisplatin-resistant tumor without regrowth. The multipronged features of light-triggered micelles represent a versatile synergistic approach for the ablation of resistant tumor in the field of cancer therapy.

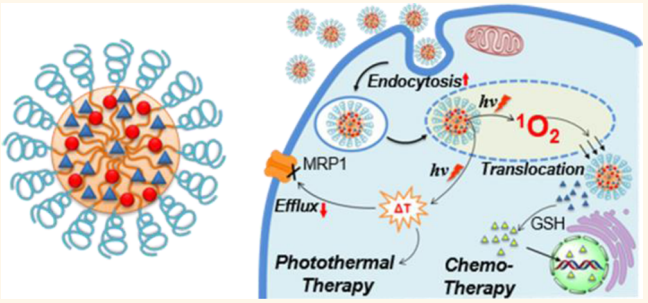

KEYWORDS: micelles · cisplatin resistance · multipronged effect · synergistic therapy · tumor ablation

Chemotherapeutic compounds are extensively used in the field of cancer therapy during past decades. However, small molecular compounds often have limited capacity for cancer therapy owing to their poor pharmacokinetics, undesirable biodistribution, insufficient intracellular delivery, and severe adverse side effects. Moreover, cancer cells frequently generate multiple drug resistance (MDR) upon chemotherapy, and thus cause chemotherapeutic failure owing to their survival from cytotoxic damage of anticancer compounds.[1] For instance, cisplatin often encounters poor therapeutic efficiency against cisplatin-resistant cancer cells, owing to insufficient accumulation at tumors, decreased cellular uptake, increased drug efflux, DNA repair, as well as metabolic modification and detoxification, resulting from the disorder of membrane protein transporters and cytoplasmic enzymes.[2−4]

To date, nanoparticles as drug vehicles have been considered as a promising platform for cancer therapy due to multiple advantages including sustained release, prolonged circulation time, enhanced permeation and retention (EPR) effect, and

* Addresses correspondence to htke@suda.edu.cn, chenhb@suda.edu.cn.

Received for review January 16, 2015 and accepted September 12, 2015.

Published online September 12, 2015
10.1021/acsnano.5b05097

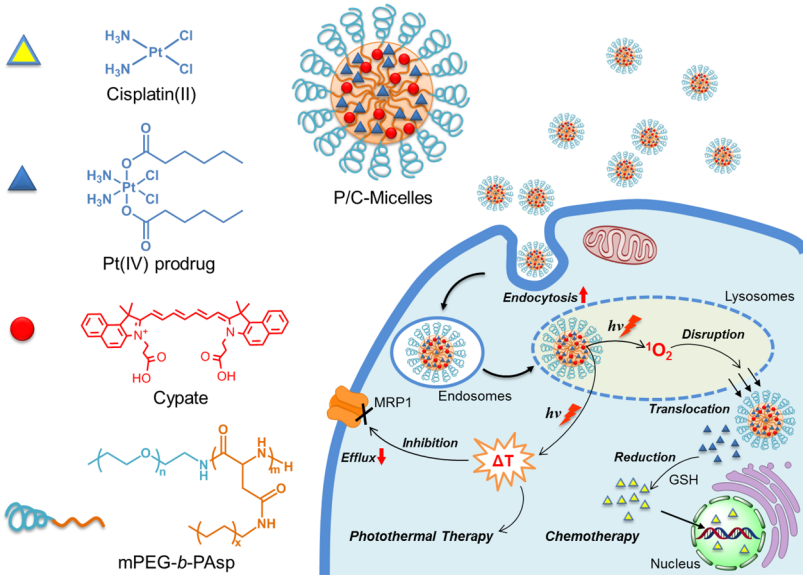

Figure 1. Schematic illustration of the micelles encapsulating Pt(IV) prodrug and Cypate (P/C-Micelles) as a multipronged nanoparticle platform for efficient ablation of resistant tumor.

superior cellular uptake, which have already facilitated the clinical development of several nanoparticles such as Genexol-PM,[5] Abraxane,[6] and SN-38.[7] In particular, various nanoparticles such as micelles, vesicles, and inorganic nanomaterials are also designed to inhibit the resistance of cancer cells to cisplatin through enhanced biodistribution and cell internalization, inhibition of drug efflux, stimuli-responsive drug release, or combinational treatments (*e.g.*, siRNA and radiation), resulting in the enhanced accessibility of cisplatin to target site or susceptibility of cancer cells.[4,8−12] Although these nanoparticles can improve physicochemical or intracellular behaviors of cisplatin including chemical stability, sustained release, cellular uptake, drug efflux, and intracellular drug translocation for inhibiting the resistance, the existing nanoparticles have limited routes to remarkably inhibit the resistance of cancer cells, resulting in the failure to ablate resistant tumor *via* intravenous administration. Consequently, it is still a major challenge to explore highly efficient nanoparticles to achieve effective therapy on the resistant tumor.

Hyperthermia as a noninvasive modality to treat cancer has been explored clinically over the past decades due to its simplicity, good efficiency, and low adverse side effects.[13−16] The hyperthermia is able to reduce cellular drug resistance through cytoplasmic protein denaturation, inhibition of DNA repair, and disturbance of signal transduction.[17−19] For instance, the hyperthermia might inhibit the overexpression of efflux transporters such as multidrug resistance-associated protein 1 (MRP1) for improving the sensitivity of resistant cancer cells to chemotherapeutic drugs.[20] Thus, the hyperthermia may potentially act as an effective approach to improve anticancer efficiency of drug against resistant cancer cells.[21−23] Recently, photothermal therapy (PTT) as an emerging strategy can achieve efficient hyperthermia by photoirradiating exogenous photoabsorbing agents such as near-infrared (NIR) cyanine dyes (*e.g.*, Cypate),[24,25] inorganic nanomaterials (*e.g.*, graphene oxide),[26,27] and gold nanoparticles,[28−31] which can effectively convert NIR light to hyperthermia for triggering cell necrosis and thus PTT efficacy. Particularly, the nanoparticles are found to improve the hyperthermia of clinically applicable cyanine dyes through enhanced biodistribution and cellular uptakes, and also facilitate the translocation of anticancer compounds into cytoplasma *via* lysosomal disruption, thereby generating enhanced photothermal or thermo-chemotherapeutic efficacy on cancer cells in our previous studies.[24,25,32] Therefore, PTT may potentially reduce the resistance of cancer cells to anticancer drug through the inhibtion of efflux transporter in addition to its photothermal damage on cancer cells owing to its hyperthermia,[33] and thus, the good photothermal conversion efficiency of photothermal agent is essential to achieve an ideal hyperthermia for desired efficacy of cisplatin on resistant tumor. Consequently, it is highly desired to constitute a nanoparticle platform integrating enhanced photothermal and chemotherapeutic features for achieving the ablation of resistant tumor.

Herein, a multipronged nanoparticle platform was rationally developed *via* the incoporation of cisplatin prodrug and cyanine dye (Cypate) into a micellar system (P/C-Micelles) for efficient ablation of cisplatin-resistant tumor (Figure 1). The micelles as an efficient vehicle exhibited the sustained release, enhanced cellular uptake, and reduced efflux of Pt(IV) prodrug and Cypate on both A549 and resistant A549R cells, as well as enhanced tumor accumulation. Meanwhile, the near-infrared light triggered an enhanced photothermal effect at pH 5.0 as compared to that at pH 7.4

owing to the enhanced nonradiative transition, which induced remarkable photothermal cytotoxicity. Moreover, the light irradiation further caused the intracellular translocation of the micelles and reduction-activable Pt(IV) prodrug into cytoplasm *via* the lysosomal disruption, as well as the inhibition on the expression of MRP1 for further reversal of drug resistance to A549R cells.[9] Consequently, the multipronged effects of light-triggered micelles generated synergistic cytotoxicity against A549R cells, and thus efficient ablation of cisplatin-resistant tumor without regrowth.

RESULTS AND DISCUSSION

Synthesis and Characterization of P/C-Micelles. To prepare P/C-Micelles, the copolymer consisting of monomethoxy poly(ethylene glycol) and decylamine-grafted poly(L-aspartic acid) (mPEG-*b*-PAsp) without hemolytic activity was synthesized *via* ring-opening polymerization of β-benzyl L-aspartate *N*-carboxyanhydride (BLA-NCA) with mPEG (12 kDa) and subsequent aminolysis of decylamine as our previous studies.[34,35] *c,t,c*-[Pt(NH$_3$)$_2$(CO$_2$CH$_2$CH$_2$CH$_2$CH$_2$ CH$_3$)$_2$Cl$_2$] (Pt(IV) prodrug) as a cisplatin prodrug[9] and photothermal Cypate were encapsulated within mPEG-*b*-PAsp to generate micellar nanoparticles for cancer-targeted delivery. The entrapment efficiencies of Pt(IV) prodrug and Cypate in P/C-Micelles were evaluated using inductively coupled plasma emission spectrometry (ICP-ES) and UV−vis spectrophotometer, respectively, indicating that 80.6 ± 3.8 wt % of Pt(IV) prodrug and 94.3 ± 1.6 wt % of Cypate were encapsulated in the micelles at the loading levels of 16.0 and 18.9% (w/w), respectively. The high loading levels might result from the good compatibility between the micellar cores with alkyl chains and the hydrophobic segments of Pt(IV) prodrug and Cypate.[25,36,37] Subsequently, P/C-Micelles were observed using transmission electron microscopy (TEM), indicating an uniform spherical morphology with diameters ranging from 60 to 100 nm (Figure 2A). Dynamic light scattering (DLS) further validated that P/C-Micelles had an average size of 81.6 ± 5.1 nm (Figure 2B), implying that the micelles with suitable size have good potential to achieve targeting capacity *via* EPR effect. Moreover, P/C-Micelles also exhibited good size stability in aqueous solutions during 9 days (Figure S1). In addition, Cypate in the

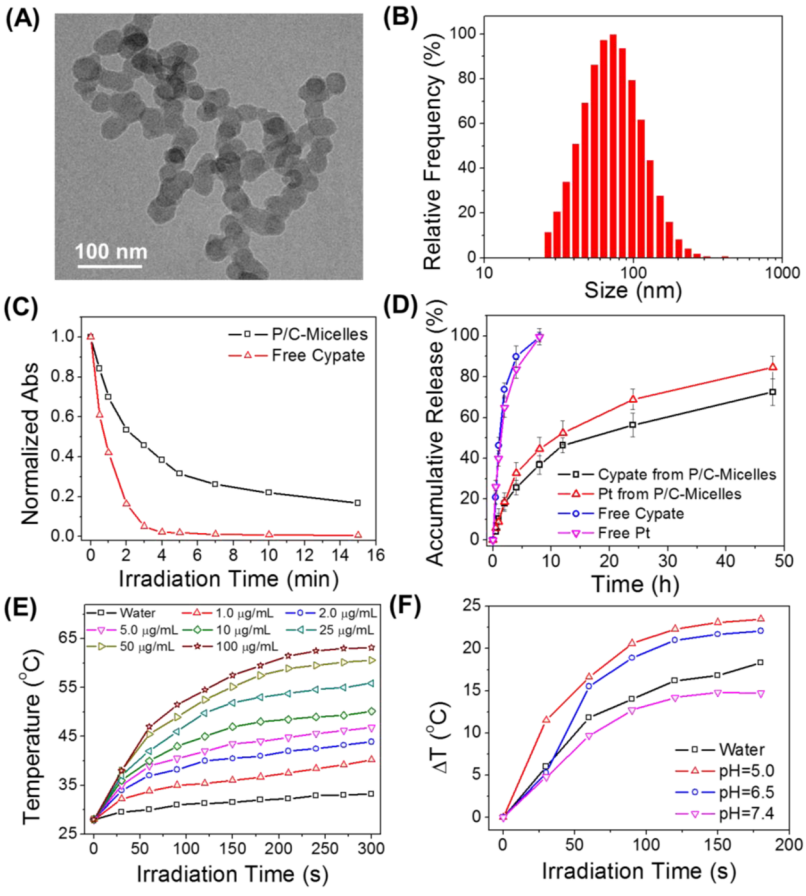

Figure 2. (A) TEM image of P/C-Micelles; (B) size distribution of P/C-Micelles; (C) normalized absorbances of P/C-Micelles and free Cypate at different time under 785 nm irradiation (1.5 W/cm^2); (D) accumulative release profiles of Cypate and Pt(IV) prodrug (Pt) from P/C-Micelles at pH 7.4; (E) temperature change of P/C-Micelles containing various concentrations of Cypate under 785 nm irradiation (1.5 W/cm^2); (F) temperature elevation of P/C-Micelles containing 10 μg/mL Cypate at various pH values.

micelles exhibited good chemical stability as compared to free Cypate (Figure S2), indicating that the micelles are able to maintain a stable nanostructure in aqueous environment.

Photostability, Drug Release, and Photothermal Effect. The photostability of P/C-Micelles was evaluated since it plays an important factor for PTT. UV−vis spectra showed that free Cypate exhibited quick decrease at absorbance upon 785 nm irradiation within 3 min, possibly owing to the rapid photobleaching (Figure 2C). However, P/C-Micelles exhibited much slower decrease in the absorbance under the same 785 nm irradiation during 15 min, indicating that the micelles can provide more efficient PTT treatment as compared to free Cypate during longer irradiation time.

Drug release plays a key prerequisite for cancer targeting. The release profiles of both Pt(IV) prodrug and Cypate in P/C-Micelles with or without 785 nm irradiation were evaluated using dialysis in PBS at pH 7.4 and 37 °C. The micelles exhibited the releases of about 18.6% Pt(IV) prodrug and 17.9% Cypate in 2 h, while free Pt(IV) prodrug (Free Pt) and free Cypate had the quick releases of 65.0 and 73.7% at pH 7.4, respectively (Figure 2D), indicating that P/C-Micelles are able to avoid burst drug release. Subsequently, P/C-Micelles exhibited continuous sustained releases of Pt(IV) prodrug and Cypate during 48 h, implying that the micelles consisting of mPEG-*b*-PAsp could significantly reduce undesirable drug release. Moreover, the micelles still exhibited the sustained releases of Pt(IV) prodrug and Cypate in fetal bovine serum as shown in Figure S3. Additionally, the acidic environment (pH 4.5) and light irradiation also had no significant influence on their sustained releases from the micelles (Figure S4).

The photothermal effects of P/C-Micelles were further evaluated by monitoring the temperature of micelles at an interval of 30 s under 785 nm irradiation at 1.5 W/cm^2 (Figure 2E). The micelles exhibited remarkable temperature increase (ΔT) ranging from 12.2 to 35.2 °C in the concentration range of 1.0−100.0 μg/mL Cypate, which is similar to that of free Cypate (Figure S5), while there was only a negligible increase in distilled water. Remarkably, P/C-Micelles as an efficient photothermal agent had a concentration-dependent photothermal effect, and easily generated the hyperthermia (above 42 °C) at relatively low concentrations,[38] which can potentially trigger photothermal damage against tumor cells. In particular, P/C-Micelles exhibited a pH-responsive photothermal effect in the range of pH 5.0−7.4 (Figure 2F). Micelles containing 10 μg/mL Cypate exhibited a remarkable increase of temperature (ΔT = 23.6 °C) at pH 5.0 during 180 s, which is much higher than that (ΔT = 13.1 °C) at pH 7.4. The enhanced photothermal effect might result from their enhanced nonradiative transition at acidic environment.[39] Reasonably, P/C-Micelles are able to induce enhanced photothermal effect at acidic environment (*e.g.*, lysosomal pH) as compared to that at pH 7.4, possibly generating stronger hyperthermia upon endocytosis into lysosomal compartments.

Cellular Uptake and Efflux. The reduced susceptibility of resistant cancer cells to anticancer compound is highly associated with several factors including defective endocytosis and down-regulation of small GTPases regulating endocytosis,[3,40] which can generally trigger a reduced internalization of cisplatin owing to decreased cellular uptake and enhanced efflux.[2,41,42] To demonstrate whether micellar nanoparticles could contribute to the internalization of Pt(IV) prodrug and Cypate by cancer cells, their cellular uptakes were evaluated in A549R and A549 cells, respectively. Figure 3A shows that the internalization of Pt(IV) prodrug from the mixture of free Pt(IV) prodrug and Cypate (free Pt/Cypate) in A549R was much less than that in A549, indicating the cellular uptake of Pt(IV) prodrug was remarkably inhibited in cisplatin-resistant cells. Interestingly, P/C-Micelles could remarkably improve cellular uptakes of Pt(IV) prodrug in both A549 and A549R cells, and there is no significant difference of cellular uptakes between A549 and A549 cells, suggesting that the micellar structure can facilitate the accumulation of Pt(IV) prodrug even in A549R cells, and impair the capacity of A549R cells to inhibit the cellular uptake of Pt(IV) prodrug. On the other hand, A549R cells exhibited no resistance to Cypate, and P/C-Micelles also improved the cellular uptakes of Cypate in both A549 and A549R cells as compared to free Cypate from free Pt/Cypate (Figure 3B). Thus, P/C-Micelles are able to facilitate the cellular uptakes of Pt(IV) prodrug and Cypate into cisplatin-resistant cancer cells for subsequent intracellular delivery.

Drug efflux plays a key role in drug resistance, and thus, the efflux of Pt(IV) prodrug within the micelles from cancer cells was further assessed as well. When A549 and A549R cells were incubated with free Pt/Cypate, the amount of excreted Pt(IV) prodrug from A549R cells was much higher than that in A549 cells, indicating the resistance of A549R cells was related to drug efflux (Figure 3C). In contrast, P/C-Micelles exhibited no significant difference of the exocytosis of Pt(IV) prodrug between A549 and A549R cells (Figure 3C), indicating the micelles as an efficient vehicle can significantly reduce drug efflux. Consequently, the micelles play a key role for enhanced internalization of Pt(IV) prodrug by the cisplatin-resistant cancer cells through their enhanced cellular uptake and reduced efflux.

Western Blotting. MDR generally involves the overexpression of efflux transporters such as MRP1. Thus, we detected the MRP1 expression levels of A549 and A549R cells treated with P/C-Micelles, free Pt/Cypate, and PBS in the presence or absence of irradiation using western blotting. After treatment with free Pt/Cypate, the expression of MRP1 in A549R cells was maintained at a high level, indicating that A549R cells remained the

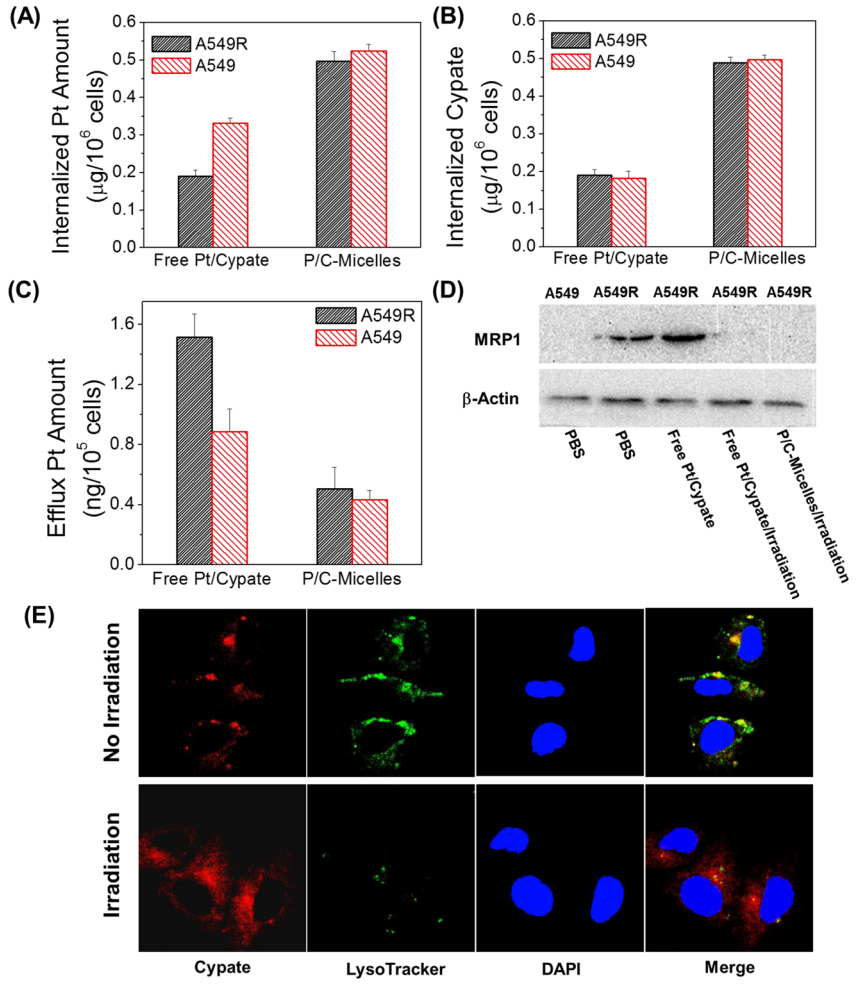

Figure 3. (A) Cellular uptakes of Pt(IV) prodrug by A549 and A549R cells after 24 h incubation with P/C-Micelles and Free Pt/Cypate, respectively; (B) cellular uptakes of Cypate by A549 and A549R cells after 24 h incubation with P/C-Micelles and Free Pt/Cypate; (C) efflux amounts of Pt(IV) prodrug from A549 and A549R cells after incubation with P/C-Micelles and Free Pt/Cypate; (D) Western blotting analysis of the MRP1 levels in A549 and A549R cells after different treatments including PBS, free Pt/Cypate, and P/C-Micelles in the presence or absence of irradiation; (E) confocal images of A549R cells treated with P/C-Micelles in the presence or absence of 3 min of irradiation (785 nm, 1.5 W/cm^2).

resistance to cisplatin (Figure 3D). However, both free Pt/Cypate and P/C-Micelles remarkably inhibited the expression levels of MRP1 under light irradiation, suggesting that hyperthermia generated from photothermal effect of Cypate upon light irradiation could further improve the susceptibility of A549R cells to drug by suppressing the resistance pathway. Reasonably, the light irradiation can remarkably inhibit the expression level of MRP1 in A549R cells *via* photothermal effect of Cypate regardless of the presence of the micelles. Therefore, the light-triggered micelles can synergistically contribute to the inhibition of drug resistance through enhanced cell internalization and reduced expression of efflux transporter.

Subcellular Distribution of P/C-Micelles. The intracellular distribution of P/C-Micelles was further evaluated using confocal laser scanning microscopy (CLSM). The lysosomes in A549R cells were stained by LysoTracker Green DND-26. As shown in Figure 3E, most of P/C-Micelles with red fluorescence from Cypate were colocalized with lysosomes when no light irradiation was carried out, indicating that P/C-Micelles can be internalized into the lysosomal compartments. However, after 3 min of irradiation, the lysosomes were mostly destructed and the red fluorescence from P/C-Micelles was mainly distributed outside lysosomes, revealing that P/C-Micelles might trigger the lysosomal disruption under light irradiation, which may potentially facilitate the translocation of drug from lysosomes into cytoplasm.

Endocytic Pathways. The endocytic pathways of P/C-Micelles were further investigated using several inhibitors of endocytosis including chlorpromazine, filipin, and amiloride (Figure 4A). It shows that chlorpromazine as an inhibitor of clathrin-mediated endocytosis resulted in the decrease of 40% cellular uptake of Pt(IV) prodrug. Obviously, P/C-Micelles possessed a clathrin-mediated endocytotic pathway in both A549 and A549R cells, which is reported to play a major role in the endocytosis of nanoparticles into cancer cells.[43] In addition, low temperature (4 °C) also induced a

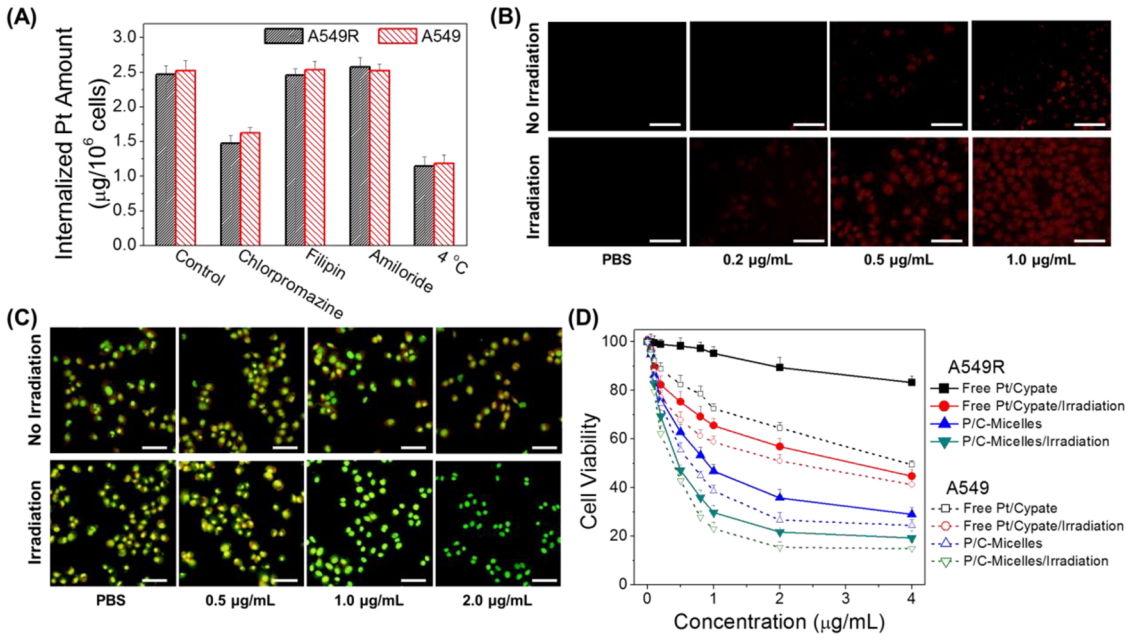

Figure 4. (A) Internalized amounts of Pt(IV) prodrug within P/C-Micelles by A549 and A549R cells treated with PBS (control), chlorpromazine (10.0 μg/mL), filipin (5.0 μg/mL), amiloride (100.0 μg/mL) at 37 °C, and PBS at 4 °C; (B) fluorescent images of A549R cells treated with P/C-Micelles for singlet oxygen detection at various doses of Cypate under irradiation or not using DHE staining (scale bar, 100 μm); (C) confocal images of lysosomal disruption of A549R cells treated with P/C-Micelles in the presence or absence of 3 min of irradiation (1.5 W/cm^2) using AO staining (scale bar, 100 μm); (D) cell viability of A549 and A549R cells treated with P/C-Micelles and free Pt/Cypate at various concentrations in the presence or absence of 1.5 W/cm^2 of irradiation (3 min).

significant decrease of cellular uptake of P/C-Micelles, indicating that the cellular uptake is also energy-dependent. The clathrin-mediated pathway allows P/C-Micelles to undergo lysosomal translocation for their intracellular delivery.

Disruption of Lysosomal Membranes through Singlet Oxygen. To validate the generation of singlet oxygen from Cypate in P/C-Micelles *via* photodynamic effect, 1, 3-diphenyliso-benzofuran (DPBF) was used as a probe to evaluate the generation of singlet oxygen from P/C-Micelles in aqueous solution, since the fluorescence of DPBF can be quenched in the presence of singlet oxygen. Figure S6 shows that P/C-Micelles began to generate detectable singlet oxygen from Cypate at a concentration of as low as 0.1 μg/mL under irradiation, and higher concentrations generated more singlet oxygen in aqueous solution, indicating a similar behavior to that of free Pt/Cypate. Obviously, the micelles avoided remarkable quenching of singlet oxygen from Cypate, possibly owing to the quick release of singlet oxygen from micellar cores into aqueous solution.[44] Next, the generation of singlet oxygen from P/C-Micelles in A549R cancer cells was observed using dihydroethidium (DHE) staining, which is able to generate red fluorescence through singlet oxygen-mediated oxidation into 2-hydroxyehtidium.[45] Figure 4B shows that the red fluorescence was generated from cancer cells treated with P/C-Micelles containing 0.2 μg/mL Cypate after irradiation, while no fluorescence was observed in the cells in the absence of irradiation. Moreover, the red fluorescence intensities were further improved when the cells suffered from P/C-Micelles containing higher Cypate concentrations, indicating that micelles possess the concentration-dependent production of intracellular singlet oxygen. The intracellular singlet oxygen from P/C-Micelles is highly potential to disrupt subcellular organelles such as lysosomes.[24,25,32]

We further observed the disruption of lysosomal membranes triggered by singlet oxygen from P/C-Micelles under irradiation using acridine orange (AO) as an intracellular indicator, which can emit red fluorescence in acidic lysosomes, and generate green fluorescence in neutralized cytosol and nuclei. The result shows that the lysosomes in A549R and A549 cells treated with PBS exhibited red fluorescence without irradiation, which was similar to those suffering from the light irradiation (Figure 4C and Figure S7). Obviously, the lysosomes remained intact in the absence of P/C-Micelles whether irradiation was present or not. However, the red fluorescence from AO was remarkably decreased in the presence of P/C-Micelles containing 0.5 μg/mL Cypate upon irradiation, and mostly disappeared at 1.0 μg/mL Cypate (Figure 4C and Figure S7). Obviously, P/C-Micelles can effectively disrupt lysosomal membranes of A549R cells even at a low concentration of Cypate under irradiation, which are able to facilitate the cytoplasmic release of both Pt(IV) prodrug and Cypate for efficient subcellular translocation in cisplatin-resistant cancer cells.

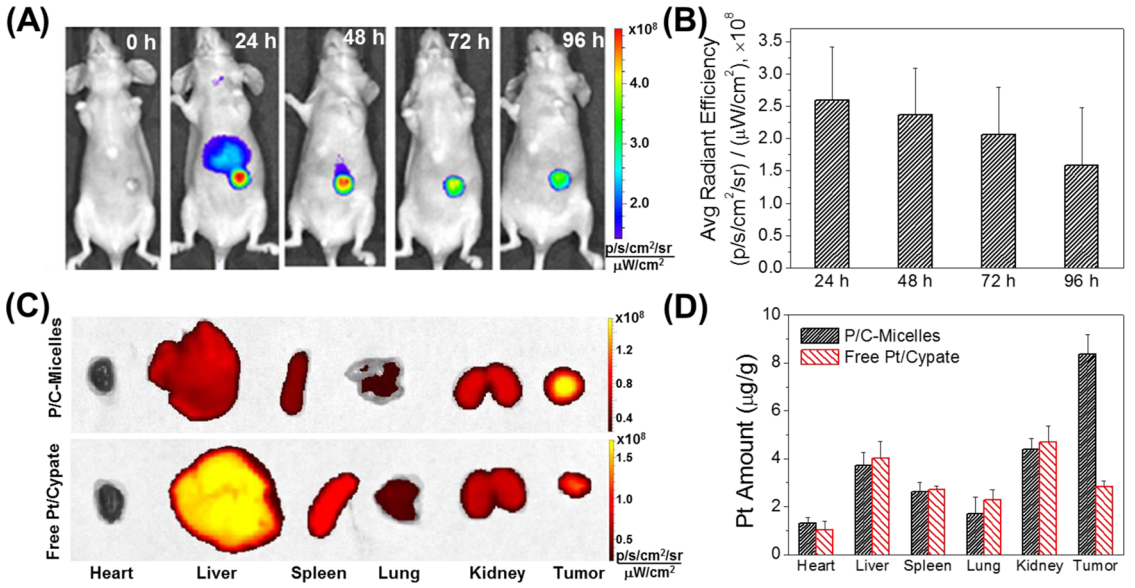

Figure 5. (A) *In vivo* NIRF imaging and (B) average NIRF intensities of the mice bearing A549R tumor injected with P/C-Micelles at the dose of 7.5 mg/kg Pt/Cypate at 0, 24, 48, 72, 96 h postinjection, (C) *ex vivo* NIRF imaging of Cypate and (D) amounts of Pt(IV) prodrug from P/C-Micelles compared to free Pt/Cypate in heart, liver, spleen, lung, kidney, and tumor of the A549R tumor bearing mice at 24 h postinjection.

Synergistic Thermo-Chemotherapeutic Cytotoxicity. The thermo-chemotherapeutic cytotoxicity of P/C-Micelles was evaluated against both A549 and A549R cells using MTT assay (Figure 4D). In our previous studies, Cypate without irradiation was found to act as a nontoxic agent without irradiation, and might not contribute to the cytotoxicity of free Pt/Cypate against the A549R and A549 cells in the absence of irradiation.[24,44] Free Pt/Cypate had an IC_{50} value of 24.7 μg/mL against A549R cells, which had a 4.7-fold increase (resistant factor, RF) as compared to that (5.2 μg/mL) against A549 cells. It indicates that A549R cells exhibit remarkable resistance to free Pt(IV) prodrug compared to A549 cells. Moreover, free Pt/Cypate exhibited the IC_{50} values of 3.0 and 2.0 μg/mL against A549R and A549 cells under irradiation, respectively, indicating a RF value of 1.50. Remarkably, free Pt/Cypate resulted in more severe cytotoxicity against both the cells *via* their thermo-chemotherapeutic effect, and the photothermal effect plays an important role in decreasing their RF value, possibly resulting from the light-triggered inhibition of MRP1.[17−23] Interestingly, P/C-Micelles exhibited more cytotoxic against both A549R cells (IC_{50}, 1.4 μg/mL) and A549 cells (IC_{50}, 1.1 μg/mL), and their RF was further decreased to as low as 1.30. The result indicates that the micelles as a nanocarrier effectively delivered Pt(IV) prodrug into the cells, which was reduced to cisplatin in cytoplasma for damaging cisplatin-resistant cells owing to its enhanced cell internalization through the enhanced cellular uptake and reduced drug efflux.[9] Most importantly, P/C-Micelles exhibited strongest cytotoxicity against both A549R cells (IC_{50}, 0.27 μg/mL) and A549 cells (IC_{50}, 0.23 μg/mL) under irradiation. Obviously, P/C-Micelles generate an effective thermo-chemotherapeutic synergy against both cancer cells under irradiation, and also resulted in the ideal RF value of 1.17, implying that the micelles could effectively overcome drug resistance *via* the synergistic cytotoxicity, possibly owing to the multipronged effects of P/C-Micelles including enhanced photostability, sustained release, pH-responsive photothermal effect, enhanced cell internalization, and chemotherapeutic damage from the micelles, as well as light-triggered hyperthermia, subcellular drug translocation, and inhibition on MRP1.

***In Vivo* NIRF Imaging and Biodistribution.** The *in vivo* NIRF cancer imaging capacity of P/C-Micelles was evaluated using the mice bearing A549R and A549 tumors. P/C-Micelles exhibited significant NIRF signals at 24 h postinjection (Figure 5A and Figure S8), indicating a good targeting capacity of P/C-Micelles. In particular, P/C-Micelles exhibited the relatively long-term retention of NIRF signals at tumors with low noises from normal tissues during the imaging period of 4 days (Figure 5B and Figure S8). The enhanced accumulations of P/C-Micelles at tumors and their quick elimination at normal tissues might provide good tumor localization with high signal-to-noise level for guiding subsequent photothermal treatment. Next, the biodistribution behavior of P/C-Micelles at 24 h postinjection was further evaluated using the mice bearing A549R and A549 tumors (Figure 5C,D, and Figure S9). P/C-Micelles exhibited 1.4-fold increase of Cypate and 2.9-fold increase of Pt(IV) prodrug in the A549R tumors as compared to free Pt/Cypate, respectively, which might result from the EPR effect of micelles. In addition, P/C-Micelles also exhibited the similar increases of accumulations of Cypate and Pt(IV) prodrug at the tumors on

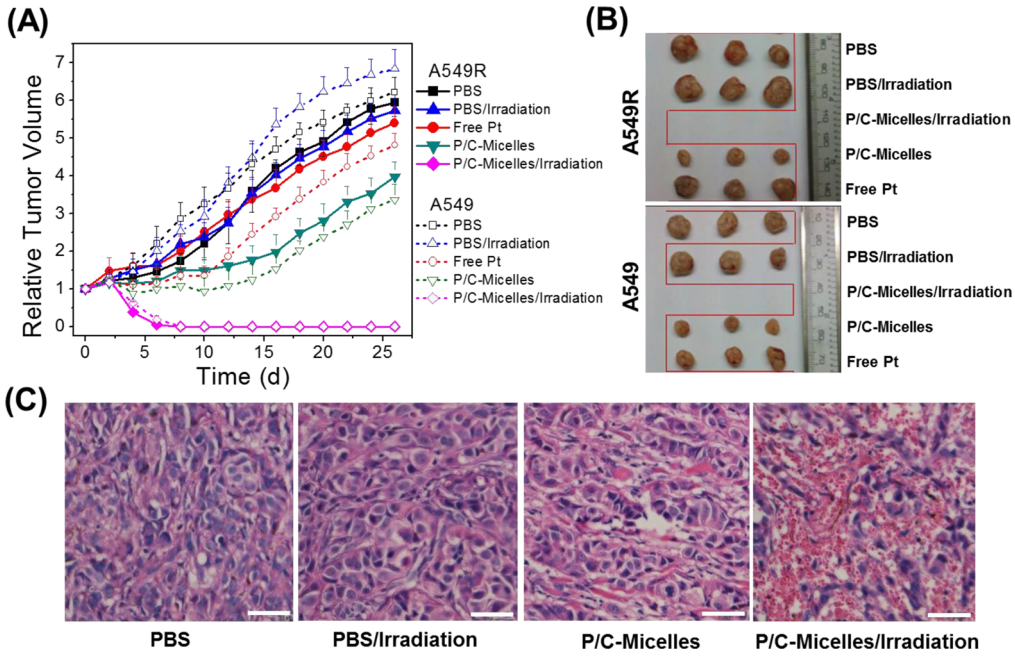

Figure 6. (A) Tumor growth profiles of the mice bearing A549R and A549 tumors treated with PBS, free Pt, and P/C-Micelles in the presence or absence of irradiation; (B) photos of the tumors extracted from the mice at the end of the experiments; (C) images of H&E-stained A549R tumor sections harvested from the mice treated with PBS and P/C-Micelles in the presence or absence of irradiation (scale bar, 50 μm).

the mice bearing A549 tumors (Figure S10). Obviously, the enhanced accumulations of P/C-Micelles at A549R tumors might facilitate synergistic thermo-chemotherapy to overcome the resistance of cancer cells.

***In Vivo* Thermo-Chemotherapeutic Synergy and *Ex Vivo* Histological Staining.** To elucidate the *in vivo* synergistic therapeutic efficacy of P/C-Micelles against cisplatin-resistant tumors under irradiation, P/C-Micelles and free Pt were intravenously injected into the mice bearing A549R tumor and A549 tumor, and then the tumors suffered from 785 nm irradiation at 24 h postinjection. Subsequently, the tumor volumes were measured for up to 26 days (Figure 6A,B). Both A549R and A549 tumors in PBS groups exhibited more than 5.7-fold increase of average tumor volumes compared to their original volumes regardless of irradiation, demonstrating that irradiation itself has a negligible influence on tumor growth. Free Pt exhibited 5.4-fold and 4.8-fold increases of tumor volumes on A549R and A549 tumors, respectively, indicating that free Pt(IV) prodrug had a slight therapeutic efficacy on both tumors, and also showed lower inhibition effect on A549R tumor owing to the drug resistance. Interestingly, P/C-Micelles without irradiation resulted in slower tumor growth behaviors on both A549R (4.0-fold increase) and A549 tumors (3.4-fold increase) compared to free Pt(IV) prodrug, respectively, revealing that their chemotherapeutic efficacy alone agrees with their enhanced cytotoxicity against A549R and A549 cells, and the micelles also play an important role in intracellular delivery of Pt(IV) prodrug for chemotherapy alone.[9] This result is also in accordance with the existing strategies to achieve enhanced therapeutic efficacy of cisplatin on resistant tumors using nanocarriers.[46] Although P/C-Micelles can exhibit the inhibition effect on A549R tumor through enhanced cellular uptake and reduced efflux, these micelles still exhibited a lower inhibition effect on A549R tumor as compared to that on A549 tumor. Remarkably, P/C-Micelles are not able to remove the whole residual resistant cancer cells surviving from chemotherapy since the tumor retains some drug resistance. Most importantly, P/C-Micelles could ablate both A549R and A549 tumors without regrowth after 8 days postirradiation, displaying a negligible difference of efficacy between A549R and A549 tumors. Remarkably, the thermo-chemotherapy of P/C-Micelles possesses synergistic effect on both tumors, and is able to ablate drug-resistant tumor through a multipronged effect from the combination of micelles and light irradiation including enhanced photostability, sustained release, pH-responsive photothermal effect, enhanced cell internalizatio, and drug accumulations at tumors, light-triggered subcellular translocation, and inhibition on the expression of MRP1, as well as simultaneous thermo-chemotherapeutic effect.[44] Thus, the multipronged effects might act as an effective strategy to ablate resistant tumor without regrowth. To the best of our knowledge, this is the first report on the ablation strategy of cisplatin-resistant tumor using nanoparticles *via* the intravenous administration.

Hematoxylin and eosin (H&E) staining of resistant A549R tumor and A549 tumor sections at 6 h postirradiation (30 h postinjection) indicates that P/C-Micelles

resulted in more severe cancer necrosis with strong hemorrhagic inflammation at both tumors under thermo-chemotherapeutic treatment (Figure 6C and Figure S11), while chemotherapy alone only caused hemorrhagic inflammation and sporadic necrotic region. PBS as a control showed no obvious tumor necrosis with or without irradiation. In addition, it also demonstrates that the micelles had no remarkable damage on heart, liver, spleen, lung, and kidney of both A549R and A549 tumor-bearing mice (Figures S12 and S13), indicating that the multipronged effects of the light-triggered micelles on tumors have low side effect on normal tissues, making it a promising strategy for the ablation of drug-resistant tumor.

CONCLUSION

In summary, P/C-Micelles were constructed *via* the encapsulation of Pt(IV) prodrug and Cypate within the copolymer of mPEG-*b*-PAsp for efficient ablation of resistant tumor. P/C-Micelles exhibited enhanced physicochemical and biological features including enhanced photostability, sustained release, pH-responsive photothermal effect, enhanced cell internalization, and tumor accumulation of the micelles, as well as light-triggered hyperthermia, subcellular drug translocation, and inhibition on expression of MRP1, which resulted in the synergistic cytotoxicity against both A549 and A549R cells. Particularly, the integration of enhanced cell internalization of the micelles and light-triggered inhibition on the expression of MRP1 plays a key role for reversing the drug resistance of A549R cells in the synergistic thermo-chemotherapy with the ablation of resistant tumor. Our strategy provides a multi-pronged approach to overcome the drug resistance for the ablation of resistant tumors in the field of cancer therapy.

METHODS

Preparation. mPEG-*b*-PAsp(DA) and Cypate were synthesized *via* a same procedure in our previous work.[24,25] *c,t,c*-[Pt(NH_3)$_2$($CO_2CH_2CH_2CH_2CH_2CH_3$)$_2$Cl$_2$] as Pt(IV) prodrug was synthesized according to the reported method.[9] For micelle preparation, mPEG-*b*-PAsp(DA) (1.2 mg), Cypate (0.4 mg), and Pt(IV) prodrug (0.4 mg) were mixed in 5 mL of methanol, and then the mixture was evaporated to generate a thin film using a rotary evaporator, followed by being dispersed using double distilled water (5.0 mL) under ultrasonication. Then, Pt(IV) prodrug/Cypate-loaded micelles (P/C-Micelles) were obtained after centrifuge separation *via* ultrafiltration (Cut-off 100 kDa). Free Pt/Cypate was obtained by simple mixing of Pt(IV) prodrug and Cypate in PBS solution.

Characterization. TEM imaging was performed using a JEOL2010 high contrast digital TEM. Particle size was measured using dynamic light scattering (Nicomp Zetasizer). The physical stability of P/C-Micelles was evaluated by monitoring their particle size during 9 days. The UV−vis absorbance and fluorescence spectra were obtained using UV−vis spectrophotometer (UV2600, Shimadzu) and fluorescence spectrophotometer (LS 55, PerkinElmer), respectively. The inductively coupled plasma emission spectrometry was used to measure the concentration of Pt(IV) prodrug. The chemical stability of P/C-Micelles was evaluated using the UV−vis assay, in which the absorbances of Cypate from the micelles and free Cypate in aqueous solutions were measured at various time.

Photostability. P/C-Micelles and free Cypate (0.5 mL, 10 μg/mL Cypate in PBS) were irradiated using a laser at 1.5 W/cm^2 (785 nm) for 0, 1, 2, 3, 5, 7, 10, and 15 min. The UV−vis absorbance spectra were measured to evaluate the absorbances of Cypate in the solutions.

Drug Release. The drug release behaviors of P/C-Micelles with or without 3 min irradiation were evaluated in the buffers at pH 7.4 and 4.5, and fetal bovine serum using dialysis method. Free Pt and free Cypate in PBS solution were used as control. The drug release was performed in a Constant Temperature Oscillator shaker at 37 °C using PBS as release medium. After the P/C-Micelles (1.0 mL) were subjected to the absence or presence of irradiation at 1.5 W/cm^2 (785 nm, 3 min), the release media were taken after 0, 1, 2, 4, 8, 12, 24, and 48 h with the replacement of an equal volume of fresh medium. UV−vis spectra and ICP-ES (ICP, Optima 8000) were performed to measure the amounts of Cypate and Pt(IV) prodrug in the samples, respectively.

Photothermal Effect. Photothermal effect was determined through the measurement of temperature under irradiation. P/C-Micelles and free Cypate in PBS (0.5 mL each) at the Cypate concentrations of 0, 1, 2, 5, 10, 25, 50, and 100 μg/mL in the plastic vials were placed under irradiation (785 nm, 1.5 W/cm^2). The temperature of solution was monitored using a thermocouple at an interval of 30 s during 300 s irradiation. The photothermal profiles of P/C-Micelles (0.5 mL, 10.0 μg/mL Cypate) were also obtained using the same procedure in various solutions including water and buffers at pH 5.0, 6.5, and 7.4.

Cellular Uptake and Efflux. A549 cells and A549R cells were seeded on 24-well culture plates (3×10^5 cells/well) and incubated overnight in DMEM containing 10% FBS. P/C-Micelles and free Pt/Cypate (4.0 μg/mL Cypate in PBS) were added for 24 h incubation, and then the cells were washed 3 times, treated with 0.5 mL of trypsin for 3 min at 37 °C, and centrifuged for cell collection and counting. Finally, the cells suffered from ultrasonication, and were treated with methanol and 1% HNO_3 to extract Cypate and Pt(IV) prodrug, followed by the analysis using UV−vis spectra and ICP-ES. In the efflux study, after 12 h incubation with P/C-Micelles and free Pt/Cypate, the A549R and A549 cells were washed three times with PBS. A half of A549R or A549 cells were harvested to measure the initial amount of Pt(IV) prodrug in the cells using ICP-ES. The other half of A549R or A549 cells were further incubated with fresh medium for additional 12 h incubation. Then, the cells were washed and further harvested to measure the final concentration of Pt(IV) prodrug using ICP-ES. The amount of efflux Pt(IV) prodrug was obtained by subtracting final amount of Pt(IV) prodrug from the initial amount of Pt(IV) prodrug.

Western Blotting. The cells were washed three times using PBS and lysed using RIPA lysis buffer supplemented with complete protease inhibitor cocktail tablets (Roche). BCA protein assay (Thermo Fisher Scientific) was used to determine protein concentration. Proteins were separated by SDS−polyacrylamide gel electrophoresis (SDS−PAGE) and transferred onto a polyvinylidene difluoride membrane (Bio-Rad). After a blocking step of 60 min with 2% BSA, the membrane was incubated with the primary antibody anti-MRP1 (Abcam) overnight at 4 °C, followed by the incubation with secondary antibody for 60 min at room temperature. The membrane was visualized using an ECL-plus detection system (GE Healthcare).

Subcellular Distribution of P/C-Micelles. Intracellular localization of P/C-Micelles in A549 cells was observed using CLSM (PE UltraView). The cells were seeded on glass slides in 35 mm dishes. Subsequently, P/C-Micelles were added into the medium for 24 h incubation. Then, Hoechst 33342 and Lysotracker Green DND-26 were coincubated for 10 min to stain the nucleus and lysosomes. Finally, the cells were observed using CLSM after 3 min in the absence or presence of irradiation (785 nm, 1.5 W/cm^2).

Endocytotic Pathways. A549 cells and A549R cells (1.2×10^6 cells/well) were seeded in 6-well plates and treated with PBS (control), and the different inhibitors including chlorpromazine (clathrin-mediated uptake, 10.0 μg/mL), amiloride (macropinocytosis, 100.0 μg/mL), and filipin (caveolae-mediated uptake, 5.0 μg/mL) in serum-free DMEM for 1 h at 37 or 4 °C, respectively. Then, P/C-Micelles (4.0 μg/mL Pt(IV) prodrug) were further added to the medium for 1 h incubation. Then, the cells were washed 3 times with PBS, treated with trypsin, centrifuged, and finally dispersed in 0.5 mL of PBS to measure Pt(IV) prodrug in the samples.

Monitoring of Singlet Oxygen. Free Cypate and P/C-Micelles containing various concentrations of Cypate in PBS (1.0 mL) containing 1, 3-diphenyliso-benzofuran (DPBF, 32 μg/mL) were irradiated for 3 min at 1.5 W/cm^2 for singlet oxygen measurement. The fluorescence spectra were measured from 450 to 565 nm at excitation wavelength of 403 nm. The DPBF solution without Cypate in the darkness was used as a control.

DHE Staining. Dihydroethidium (DHE) was used as an indicator of reactive oxygen species (ROS) formation. A549 and A549R cells were seeded on 24-well plates at the density of 3×10^5 per well and incubated with P/C-Micelles containing 0.2, 0.5, and 1.0 μg/mL Cypate for 6 h. The cells were washed 3 times using PBS, and 0.2 mL of DHE solution (5 μM in PBS) was added to the wells for 30 min incubation at 37 °C, followed by treatment with or without irradiation (3 min, 785 nm, 1.5 W/cm^2). Subsequently, the cells were washed and imaged using an inverted fluorescent microscope with the excitation of green light.

Disruption of Lysosomal Membranes. Acridine orange (AO) was used as an intracellular indicator of acidic organelle integrity in A549 and A549R cells. A549 and A549R cells were seeded overnight in 24-well plates and treated with PBS and P/C-Micelles at Cypate concentrations of 0, 0.5, 1.0, and 2.0 μg/mL for 6 h. Then, fresh medium was added, followed by 3 min irradiation at 1.5 W/cm^2. After another 1 h incubation, A549 and A549R cells were washed using PBS and further incubated with AO (1.0 mL, 6 μM) for 15 min. Subsequently, the cells were washed 3 times using PBS and then were observed using fluorescence microscopy (IX 51, Olympus) with the excitation wavelength of 488 nm, and emission wavelengths ranging from 515 to 545 nm (green) and from 610 to 640 nm (red).

MTT Assay. A549 cells and A549R cells were incubated in 96-well plates at 37 °C for 24 h. Free Pt/Cypate and P/C-Micelles were incubated with cells for 24 h at different doses including 0, 0.005, 0.1, 0.2, 0.5, 0.8, 1.0, 2.0, and 4.0 μg/mL Cypate. Then, the cells were washed using PBS, irradiated at 785 nm for 3 min at 1.5 W/cm^2. After another incubation of 24 h, the cell viabilities were determined using MTT assay.

Biodistribution. A549 cells and A549R cells (1×10^7 cells) were subcutaneously injected into the flanks of female BALB/c nude mice (16−18 g) to obtain the tumor-bearing mice. Free Pt/Cypate and P/C-Micelles were intravenously injected at the dose of 7.5 mg/kg Cypate. Then, the tissues including heart, liver, spleen, lung, kidney, and tumor were extracted from the mice at 24 h postinjection. The extracted tissues were imaged using IVIS Lumina II with the excitation wavelength of 785 nm. The NIRF signals in the tissues were calculated to describe the *ex vivo* biodistribution of Cypate at 24 h postinjection. Subsequently, the tissues were further homogenized, centrifuged, and extracted using 2.0 mL of HNO_3 for the measurement of Pt(IV) prodrug using ICP-ES.

***In Vivo* Imaging.** A549 and A549R cells (1×10^7 cells) were separately subcutaneously injected into the flanks of female BALB/c nude mice (16−18 g) to obtain the A549 and A549R tumor-bearing mice. Free Cypate and P/C-Micelles were intravenously injected into the mice at the dose of 7.5 mg/kg Cypate. Then, the mice were imaged through IVIS Lumina II with the excitation wavelength of 785 nm at 24, 48, 72, and 96 h postinjection. The average NIRF intensities of the tumors were calculated to describe the photon signals at tumor at different time.

***In Vivo* Efficacy.** A549 cells and A549R cells (1×10^7 cells) were subcutaneously transplanted into the flanks of female mice until the tumor size reaches approximately 50−70 mm^3 (about 10 days after transplantation). Tumor volumes were measured using a caliper according to the equation of $V = 0.5 \times a \times b^2$ (where a and b are the long and short diameters of tumor, respectively). Various formulations including PBS, free Pt, and P/C-Micelles were injected intravenously into the mice at the dose of 7.5 mg/kg Cypate or 7.5 mg/kg Pt(IV) prodrug on day 0, 2, and 4. Subsequently, the tumors treated with PBS and P/C-Micelles were irradiated for 3 min (785 nm, 1.5 W/cm^2) or not at 24 h postinjection. Then, the tumor volumes were measured and normalized against the original volumes (0 day). Finally, the mice were sacrificed by cervical dislocation under an anesthetic status after the experiments.

***Ex Vivo* Histological Staining.** The A549 tumor-bearing mice were injected with PBS and P/C-Micelles at the dose of 7.5 mg/kg Cypate or 7.5 mg/kg Pt(IV) prodrug, and then the tumors (~60 mm^3) were irradiated for 3 min (785 nm, 1.5 W/cm^2) at 24 h postinjection. Next, the tissues including heart, liver, spleen, lung, kidney, and tumor were dissected from mice at 6 h postirradiation (30 h postinjection), and then fixed in a 4% formaldehyde solution for 24 h at room temperature. The sections of 10 μm in thickness were obtained after the tissues were frozen. Finally, H&E staining was performed, and the sections were observed using an Olympus IX73 bright field microscope.

Conflict of Interest: The authors declare no competing financial interest.

Supporting Information Available: The Supporting Information is available free of charge on the ACS Publications website at DOI: 10.1021/acsnano.5b05097.

Additional figures of size stability, chemical stability, drug release, photothermal profiles, singlet oxygen generation, lysosomal disruption observation, *in vivo* NIRF imaging, tissue distribution, and H&E-staining (PDF)

Acknowledgment. This work was supported by National Natural Science Foundation of China (31422021, 51473109, 31500811 and 81501585), National Basic Research Program (2012CB932500 and 2014CB931903), the Priority Academic Program Development of Jiangsu Higher Education Institutions (PAPD), and Jiangsu Key Laboratory of Translational Research and Therapy for Neuro-Psycho-Diseases.

REFERENCES AND NOTES

1. Holohan, C.; Van Schaeybroeck, S.; Longley, D. B.; Johnston, P. G. Cancer Drug Resistance: an Evolving Paradigm. *Nat. Rev. Cancer* **2013**, *13*, 714–726.
2. Kartalou, M.; Essigmann, J. M. Mechanisms of Resistance to Cisplatin. *Mutat. Res., Fundam. Mol. Mech. Mutagen.* **2001**, *478*, 23–43.
3. Stewart, D. J. Mechanisms of Resistance to Cisplatin and Carboplatin. *Crit. Rev. Oncol. Hematol.* **2007**, *63*, 12–31.
4. Xue, X.; Hall, M. D.; Zhang, Q.; Wang, P. C.; Gottesman, M. M.; Liang, X. J. Nanoscale Drug Delivery Platforms Overcome Platinum-Based Resistance in Cancer Cells due to Abnormal Membrane Protein Trafficking. *ACS Nano* **2013**, *7*, 10452–10464.
5. Kim, T. Y.; Kim, D. W.; Chung, J. Y.; Shin, S. G.; Kim, S. C.; Heo, D. S.; Kim, N. K.; Bang, Y. J. Phase I and Pharmacokinetic Study of Genexol-PM, A Cremophor-Free, Polymeric Micelle-Formulated Paclitaxel, in Patients with Advanced Malignancies. *Clin. Cancer Res.* **2004**, *10*, 3708–3716.
6. Green, M. R.; Manikhas, G. M.; Orlov, S.; Afanasyev, B.; Makhson, A. M.; Bhar, P.; Hawkins, M. J. Abraxane. A Novel Cremophor-Free, Albumin-Bound Particle Form of Paclitaxel for the Treatment of Advanced Non-Small-Cell Lung Cancer. *Ann. Oncol.* **2006**, *17*, 1263–1268.
7. Kawato, Y.; Aonuma, M.; Hirota, Y.; Kuga, H.; Sato, K. Intracellular Roles of SN-38, A Metabolite of the Camptothecin Derivative CPT-11, in the Antitumor Effect of CPT-11. *Cancer Res.* **1991**, *51*, 4187–4191.
8. Liang, X. J.; Meng, H.; Wang, Y.; He, H.; Meng, J.; Lu, J.; Wang, P. C.; Zhao, Y.; Gao, X.; Sun, B.; et al. Metallofullerene Nanoparticles Circumvent Tumor Resistance to Cisplatin by Reactivating Endocytosis. *Proc. Natl. Acad. Sci. U. S. A.* **2010**, *107*, 7449–7454.

9. Dhar, S.; Gu, F. X.; Langer, R.; Farokhzad, O. C.; Lippard, S. J. Targeted Delivery of Cisplatin to Prostate Cancer Cells by Aptamer Functionalized Pt(IV) Prodrug-PLGA-PEG Nanoparticles. *Proc. Natl. Acad. Sci. U. S. A.* **2008**, *105*, 17356–17361.
10. Graf, N.; Bielenberg, D. R.; Kolishetti, N.; Muus, C.; Banyard, J.; Farokhzad, O. C.; Lippard, S. J. Alpha(V)Beta(3) Integrin-Targeted PLGA-PEG Nanoparticles for Enhanced Anti-Tumor Efficacy of a Pt(IV) Prodrug. *ACS Nano* **2012**, *6*, 4530–4539.
11. Min, Y.; Mao, C. Q.; Chen, S.; Ma, G.; Wang, J.; Liu, Y. Combating the Drug Resistance of Cisplatin using a Platinum Prodrug Based Delivery System. *Angew. Chem., Int. Ed.* **2012**, *51*, 6742–6747.
12. Ito, M.; Yamamoto, S.; Nimura, K.; Hiraoka, K.; Tamai, K.; Kaneda, Y. Rad51 siRNA Delivered by HVJ Envelope Vector Enhances the Anti-Cancer Effect of Cisplatin. *J. Gene Med.* **2005**, *7*, 1044–1052.
13. Kim, J. H.; Hahn, E. W.; Tokita, N. Combination Hyperthermia and Radiation Therapy for Cutaneous Malignant Melanoma. *Cancer* **1978**, *41*, 2143–2148.
14. Corry, P. M.; Barlogie, B.; Tilchen, E. J.; Armour, E. P. Ultrasound-Induced Hyperthermia for the Treatment of Human Superficial Tumors. *Int. J. Radiat. Oncol., Biol., Phys.* **1982**, *8*, 1225–1229.
15. Arcangeli, G.; Barni, E.; Cividalli, A.; Mauro, F.; Morelli, D.; Nervi, C.; Spano, M.; Tabocchini, A. Effectiveness of Microwave Hyperthermia Combined with Ionizing Radiation: Clinical Results on Neck Node Metastases. *Int. J. Radiat. Oncol., Biol., Phys.* **1980**, *6*, 143–148.
16. Brusentsov, N. A.; Nikitin, L. V.; Brusentsova, T. N.; Kuznetsov, A. A.; Bayburtskiy, F. S.; Shumakov, L. I.; Jurchenko, N. Y. Magnetic Fluid Hyperthermia of the Mouse Experimental Tumor. *J. Magn. Magn. Mater.* **2002**, *252*, 378–380.
17. Hettinga, J. V.; Konings, A. W.; Kampinga, H. H. Reduction of Cellular Cisplatin Resistance by Hyperthermia - a Review. *Int. J. Hyperthermia* **1997**, *13*, 439–457.
18. Eichholtz-Wirth, H.; Hietel, B. Heat Sensitization to Cisplatin in Two Cell Lines with Different Drug Sensitivities. *Int. J. Hyperthermia* **1990**, *6*, 47–55.
19. Chu, K. F.; Dupuy, D. E. Thermal Ablation of Tumours: Biological Mechanisms and Advances in Therapy. *Nat. Rev. Cancer* **2014**, *14*, 199–208.
20. Souslova, T.; Averill-Bates, D. A. Multidrug-Resistant HeLa Cells Overexpressing MRP1 Exhibit Sensitivity to Cell Killing by Hyperthermia: Interactions with Etoposide. *Int. J. Radiat. Oncol., Biol., Phys.* **2004**, *60*, 1538–1551.
21. Hauck, T. S.; Jennings, T. L.; Yatsenko, T.; Kumaradas, J. C.; Chan, W. C. W. Enhancing the Toxicity of Cancer Chemotherapeutics with Gold Nanorod Hyperthermia. *Adv. Mater.* **2008**, *20*, 3832–3838.
22. Los, G.; Sminia, P.; Wondergem, J.; Mutsaers, P. H.; Havemen, J.; ten Bokkel Huinink, D.; Smals, O.; Gonzalez-Gonzalez, D.; McVie, J. G. Optimisation of Intraperitoneal Cisplatin Therapy with Regional Hyperthermia in Rats. *Eur. J. Cancer Clin. Oncol.* **1991**, *27*, 472–477.
23. Atmaca, A.; Al-Batran, S. E.; Neumann, A.; Kolassa, Y.; Jager, D.; Knuth, A.; Jager, E. Whole-Body Hyperthermia (WBH) in Combination with Carboplatin in Patients with Recurrent Ovarian Cancer - A Phase II Study. *Gynecol. Oncol.* **2009**, *112*, 384–388.
24. Yang, H.; Mao, H.; Wan, Z.; Zhu, A.; Guo, M.; Li, Y.; Li, X.; Wan, J.; Yang, X.; Shuai, X.; et al. Micelles Assembled with Carbocyanine Dyes for Theranostic Near-Infrared Fluorescent Cancer Imaging and Photothermal Therapy. *Biomaterials* **2013**, *34*, 9124–9133.
25. Guo, M.; Mao, H.; Li, Y.; Zhu, A.; He, H.; Yang, H.; Wang, Y.; Tian, X.; Ge, C.; Peng, Q.; et al. Dual Imaging-Guided Photothermal/Photodynamic Therapy using Micelles. *Biomaterials* **2014**, *35*, 4656–4666.
26. Robinson, J. T.; Tabakman, S. M.; Liang, Y.; Wang, H.; Casalongue, H. S.; Vinh, D.; Dai, H. Ultrasmall Reduced Graphene Oxide with High Near-Infrared Absorbance for Photothermal Therapy. *J. Am. Chem. Soc.* **2011**, *133*, 6825–6831.
27. Yang, K.; Zhang, S.; Zhang, G.; Sun, X.; Lee, S. T.; Liu, Z. Graphene in Mice: Ultrahigh *in Vivo* Tumor Uptake and Efficient Photothermal Therapy. *Nano Lett.* **2010**, *10*, 3318–3323.
28. O'Neal, D. P.; Hirsch, L. R.; Halas, N. J.; Payne, J. D.; West, J. L. Photo-Thermal Tumor Ablation in Mice using Near Infrared-Absorbing Nanoparticles. *Cancer Lett.* **2004**, *209*, 171–176.
29. Melancon, M. P.; Zhou, M.; Li, C. Cancer Theranostics with Near-Infrared Light-Activatable Multimodal Nanoparticles. *Acc. Chem. Res.* **2011**, *44*, 947–956.
30. Rai, P.; Mallidi, S.; Zheng, X.; Rahmanzadeh, R.; Mir, Y.; Elrington, S.; Khurshid, A.; Hasan, T. Development and Applications of Photo-Triggered Theranostic Agents. *Adv. Drug Delivery Rev.* **2010**, *62*, 1094–1124.
31. Huang, X.; El-Sayed, I. H.; Qian, W.; El-Sayed, M. A. Cancer Cell Imaging and Photothermal Therapy in the Near-Infrared Region by Using Gold Nanorods. *J. Am. Chem. Soc.* **2006**, *128*, 2115–2120.
32. Chen, H.; Xiao, L.; Anraku, Y.; Mi, P.; Liu, X.; Cabral, H.; Inoue, A.; Nomoto, T.; Kishimura, A.; Nishiyama, N.; et al. Polyion Complex Vesicles for Photoinduced Intracellular Delivery of Amphiphilic Photosensitizer. *J. Am. Chem. Soc.* **2014**, *136*, 157–163.
33. Zheng, M.; Yue, C.; Ma, Y.; Gong, P.; Zhao, P.; Zheng, C.; Sheng, Z.; Zhang, P.; Wang, Z.; Cai, L. Single-Step Assembly of DOX/ICG Loaded Lipid--Polymer Nanoparticles for Highly Effective Chemo-Photothermal Combination Therapy. *ACS Nano* **2013**, *7*, 2056–2067.
34. Anraku, Y.; Kishimura, A.; Oba, M.; Yamasaki, Y.; Kataoka, K. Spontaneous Formation of Nanosized Unilamellar Polyion Complex Vesicles with Tunable Size and Properties. *J. Am. Chem. Soc.* **2010**, *132*, 1631–1636.
35. Anraku, Y.; Kishimura, A.; Kobayashi, A.; Oba, M.; Kataoka, K. Size-Controlled Long-Circulating Picsome as a Ruler to Measure Critical Cut-Off Disposition Size into Normal and Tumor Tissues. *Chem. Commun.* **2011**, *47*, 6054–6056.
36. Altnoğlu, E. I.; Russin, T. J.; Kaiser, J. M.; Barth, B. M.; Eklund, P. C.; Kester, M.; Adair, J. H. Near-Infrared Emitting Fluorophore-Doped Calcium Phosphate Nanoparticles for *In Vivo* Imaging of Human Breast Cancer. *ACS Nano* **2008**, *2*, 2075–2084.
37. Miki, K.; Kimura, A.; Oride, K.; Kuramochi, Y.; Matsuoka, H.; Harada, H.; Hiraoka, M.; Ohe, K. High-Contrast Fluorescence Imaging of Tumors *in Vivo* Using Nanoparticles of Amphiphilic Brush-Like Copolymers Produced by ROMP. *Angew. Chem., Int. Ed.* **2011**, *50*, 6567–6570.
38. Hahn, G. M.; Braun, J.; Har-Kedar, I. Thermochemotherapy: Synergism between Hyperthermia (42−43 Degrees) and Adriamycin (of Bleomycin) in Mammalian Cell Inactivation. *Proc. Natl. Acad. Sci. U. S. A.* **1975**, *72*, 937–940.
39. Guo, M.; Huang, J.; Deng, Y.; Shen, H.; Ma, Y.; Zhang, M.; Zhu, A.; Li, Y.; Hui, H.; Wang, Y.; et al. pH-Responsive Cyanine-Grafted Graphene Oxide for Fluorescence Resonance Energy Transfer-Enhanced Photothermal Therapy. *Adv. Funct. Mater.* **2015**, *25*, 59–67.
40. Shen, D. W.; Su, A.; Liang, X. J.; Pai-Panandiker, A.; Gottesman, M. M. Reduced Expression of Small GTPases and Hypermethylation of the Folate Binding Protein Gene in Cisplatin-Resistant Cells. *Br. J. Cancer* **2004**, *91*, 270–276.
41. Andrews, P. A.; Howell, S. B. Cellular Pharmacology of Cisplatin: Perspectives on Mechanisms of Acquired Resistance. *Cancer Cells* **1990**, *2*, 35–43.
42. Dempke, W. C.; Shellard, S. A.; Hosking, L. K.; Fichtinger-Schepman, A. M.; Hill, B. T. Mechanisms Associated with the Expression of Cisplatin Resistance in a Human Ovarian Tumor Cell Line Following Exposure to Fractionated X-Irradiation in Vitro. *Carcinogenesis* **1992**, *13*, 1209–1215.
43. Iversen, T.-G.; Skotland, T.; Sandvig, K. Endocytosis and Intracellular Transport of Nanoparticles: Present Knowledge and Need for Future Studies. *Nano Today* **2011**, *6*, 176–185.
44. Wan, Z.; Mao, H.; Guo, M.; Li, Y.; Zhu, A.; Yang, H.; He, H.; Shen, J.; Zhou, L.; Jiang, Z.; et al. Highly Efficient Hierarchical Micelles Integrating Photothermal Therapy

and Singlet Oxygen-Synergized Chemotherapy for Cancer Eradication. *Theranostics* **2014**, *4*, 399–411.
45. Pan, Y.; Schroeder, E. A.; Ocampo, A.; Barrientos, A.; Shadel, G. S. Regulation of Yeast Chronological Life Span by TORC1 *via* Adaptive Mitochondrial ROS Signaling. *Cell Metab.* **2011**, *13*, 668–678.
46. Yang, X. Z.; Du, X. J.; Liu, Y.; Zhu, Y. H.; Liu, Y. Z.; Li, Y. P.; Wang, J. Rational Design of Polyion Complex Nanoparticles to Overcome Cisplatin Resistance in Cancer Therapy. *Adv. Mater.* **2014**, *26*, 931–936.